Journal of Catalysis **187,** 1–14 (1999)
Article ID jcat.1999.2578, available online at http://www.idealibrary.com on IDEAL®

$CuO–SiO_2$ Sol–Gel Catalysts: Characterization and Catalytic Properties for NO Reduction

G. Díaz,[1] R. Pérez-Hernández, A. Gómez-Cortés, M. Benaissa, R. Mariscal,* and J. L. G. Fierro*

*Depto. Física Química, Instituto de Física UNAM, P.O. Box 20-364, Mexico 01000; and *Instituto de Catálisis y Petroleoquímica, CSIC, Cantoblanco, 28049 Madrid, Spain*

Received August 27, 1998; revised May 28, 1999; accepted May 28, 1999

$CuO–SiO_2$ catalysts were prepared by the sol–gel technique and calcined at two temperatures, 673 and 1073 K. Characterization of the catalysts was achieved by BET, FTIR, TPR, dissociative N_2O adsorption, XPS, HRTEM, and reactivity toward $NO + H_2$. As a function of the calcination temperature, characterization techniques showed: textural (BET), morphological and structural (HRTEM), reducibility (TPR, XPS), dispersion, and catalytic reactivity ($NO + H_2$) differences between samples. Both samples showed remarkable stability during on-stream experiments. The microstructure of the catalysts as a consequence of the preparation method allows the understanding of the catalytic behavior of calcined and reduced samples as well as the stability toward sintering.

Key Words: **$CuO–SiO_2$ sol–gel; characterization by physical and chemical techniques; NO reduction.**

1. INTRODUCTION

Nitrogen oxide reduction by catalytic means is one of the most important reactions under research due to its importance in the control of atmospheric pollution. Currently, the catalytic converters in automobiles contain Rh, Pt, and Pd supported on a ceramic monolith (1); nevertheless the high demand of rhodium in contrast to its small supply in nature has led to increased efforts to find alternative more abundant materials and less expensive replacements. One of these options is copper-based catalysts. The selective catalytic reduction of NO over Cu-containing zeolites has been the subject of intense research in the past years, driven by the expectations of large-scale applications for the control of NO_x (2).

The catalytic behavior of supported copper oxide is influenced by the nature of the support, the dispersion of copper, and the surface changes occurring during the catalytic reaction and redox cycles. The nature of the surface copper species depends on the loading and calcination temperatures. Shimokawabe *et al.* (3) reported for silica-supported copper catalysts prepared by ionic exchange the presence of isolated copper ions and highly dispersed Cu^{+2} clusters for samples calcined between 673 and 873 K. The ion exchange method stabilizes copper species on silica. The Cu^{+2} clusters crystallize to bulk CuO above 973 K, whereas bulk CuO is already obtained at 773 K when copper is impregnated on silica. The various copper surface species are characterized by different reducibility properties. De Jong *et al.* (4) observed that the particle size and shape of copper particles deposited on silica can be modified by repeated redox cycles. van der Grift *et al.* (5) noted that depending on the severity of the reduction treatment, the structure of the copper particles on silica suffered changes from an atomically rough surface to a stepped one and finally to a densely packed surface. These surface changes are reversible as long as the particle size is not increased.

Stabilization of the active phase in supported catalysts depends on the support and the preparation method. Among the preparation methods for copper catalysts, the sol–gel technique offers some advantages. With this preparation method, copper species are effectively incorporated into the ionic oxide network (6) and may lead to more stable catalysts than those prepared by conventional methods. The sol–gel polymerization of metal alkoxides in the presence of inorganic salts leads to the formation of ceramic oxide materials that exhibit important microstructure properties (7).

Accordingly, this work was undertaken with the aim of exploring the capability of the sol–gel method for the preparation of $CuO–SiO_2$ catalysts and to see whether such a method can yield copper species stabilized by the carrier. Characterization of the catalyst structures by several physical and chemical techniques, including BET measurements, infrared spectroscopy, temperature-programmed reduction, dissociative N_2O adsorption, X-ray photoelectron spectroscopy, and high resolution transmission electron microscopy, has been used to correlate the microstructure of the solids with their catalytic performance in the NO reduction by hydrogen.

2. EXPERIMENTAL

2.1. Catalyst Preparation

Samples were prepared by the sol–gel method from $Si(OC_2H_5)_4$ (TEOS) and $Cu(CH_3COO)_2H_2O$ precursors

0021-9517/99 $30.00

according to (8). The CuO content was 5.0 mol%. TEOS was first partially hydrolyzed at reflux temperature using NH_4OH as the catalyst and ethanol as the solvent. The molar ratio $TEOS/C_2H_5OH/H_2O/NH_4OH$ was at this time 1:4:1:0.33 and there was Cu $(CH_3COO)_2H_2O$ in the right amount to get the nominal CuO content. After 10 min at reflux temperature, 3 mol of H_2O was added to complete hydrolysis and reflux was continued for another 50 min. The resultant mixture was aged for 24 h and the residual liquid was then removed by decanting. The xerogel (CSSX) was obtained after heating at 353 K for 24 h. Aliquots of the xerogel were calcined in air at 673 and 1073 K for 72 h. Each aliquot was heated at a rate of 5 K/min from room temperature to 373 K where it was held for 1 h. The temperature was then increased at the same rate to reach the calcination temperature (673 or 1073 K). Hereafter, catalysts will be referred as CSS4 and CSS8 for samples calcined at 673 and 1073 K, respectively.

2.2. Catalyst Characterization

The chemical transformations of the catalyst precursors brought about by calcination temperature were followed by FTIR (from treated materials) using a Nicolet-5SX spectrometer. Standard procedures were used for sample preparation; the sample was diluted in KBr (1/1000), crushed in an agate mortar, and pressed into thin disks. Spectra were recorded in the 4000 to 300 cm^{-1} range working with a resolution of 4 cm^{-1}.

The TPR experiments and the surface area determination were done in a multitask characterization unit RIG-100 from In-Situ Research Instruments Inc. For TPR runs, experimental conditions were chosen according to the literature (9). The sample (0.1 g) was placed in the reactor, purged with He at room temperature, and then heated at a rate of 10 K/min in the presence of a 5% H_2/Ar gas mixture (30 cm^3/min). Total surface area was determined by the single-point method using a 30% N_2/He gas mixture.

The number of surface Cu sites for TON evaluation was determined by dissociative N_2O adsorption at 363 K using the procedure described by van der Grift *et al.* (5). The catalysts were first reduced at 773 K for 1 h. Afterward, they were flushed with Ar and temperature was decreased to 363 K. Then, N_2O was admitted to the reactor at this temperature and allowed to flow (50 cm^3/min) for 45 min. Finally, the samples were again flushed with Ar and cooled to room temperature in order to start a TPR run.

The HRTEM microstructure characterization of the solids was achieved in a JEOL 4000EX electron microscope and electron micrographs were recorded at a magnification of 600,000×. Samples were supported on holey carbon grids by simply grinding the specimen between two glass plates and bringing the powder in contact with the grid.

X-ray photoelectron spectra were obtained using a VG ESCALAB 200R spectrometer equipped with a Mg$K\alpha$ X-ray radiation source ($h\nu = 1253.6$ eV) and a hemispherical electron analyzer. The powder samples were pressed into small stainless steel cylinders and then were outgassed in the pretreatment chamber of the spectrometer up to 10^{-9} Torr prior to transfer to the analysis chamber. The Si 2p peak with a BE of 103.4 eV was chosen as an internal reference (10). This reference was in all cases in good agreement with the BE of the C 1s peak, arising from contamination, at 284.9 eV. This reference gave an accuracy of ±0.1 eV.

2.3. Catalytic Activity Measurements

The reduction of nitric oxide was studied in the temperature range 373–873 K using a commercial flow system (RIG-100, In Situ Research Instruments Inc.) working at atmospheric pressure. The NO/H_2 molar ratio was 1 and 0.5 and the GHSV = 20,000 h^{-1}. The reactant mixture (balance He 98 vol%) was fed to the microreactor at room temperature after the system was purged in He. The reactor temperature was then increased to reach 373 K and catalytic activity measurements initiated. For each temperature that was considered, the catalytic activity determinations were done at the steady state. Total activity was followed by the NO consumption as a function of the reaction temperature according to $\%\alpha_{NO} = \{[[NO]_{in} - [NO]_{out}]/[NO]_{in}\}(100)$, where $[NO]_{in}$ and $[NO]_{out}$ are the NO concentration at the inlet and at the exit of the reactor, respectively. The selectivity in mol% was calculated as $\%S_i = [C_i/\sum C_i](\%\ \alpha_{NO})$.

The reaction products were analyzed by gas chromatography using TCD. A 4-m packed Chromosorb 103 column was used to separate products coming from the $NO + H_2$ reaction: N_2 and NO were separated at 303 K, and N_2O, NH_3, and H_2O at 403 K. Calibration for quantitative analysis was performed using pure gases. Estimated error in activity and selectivity data is in the range ≤5%.

3. RESULTS

Surface Area (BET)

BET surface areas of the xerogel and the CSS4 and CSS8 samples are compiled in Table 1. Calcination of the xerogel (CSSX) at moderately low temperature (673 K) led to the development of a high surface area in the sample. The

TABLE 1

BET Surface Area of $CuO–SiO_2$ Catalysts

Sample	Surface area (m^2/g)
XCSS	245
CSS4	312
CSS8	155

Note. XCSS, xerogel; CSS4, xerogel calcined at 673 K; CSS8, xerogel calcined at 1073 K.

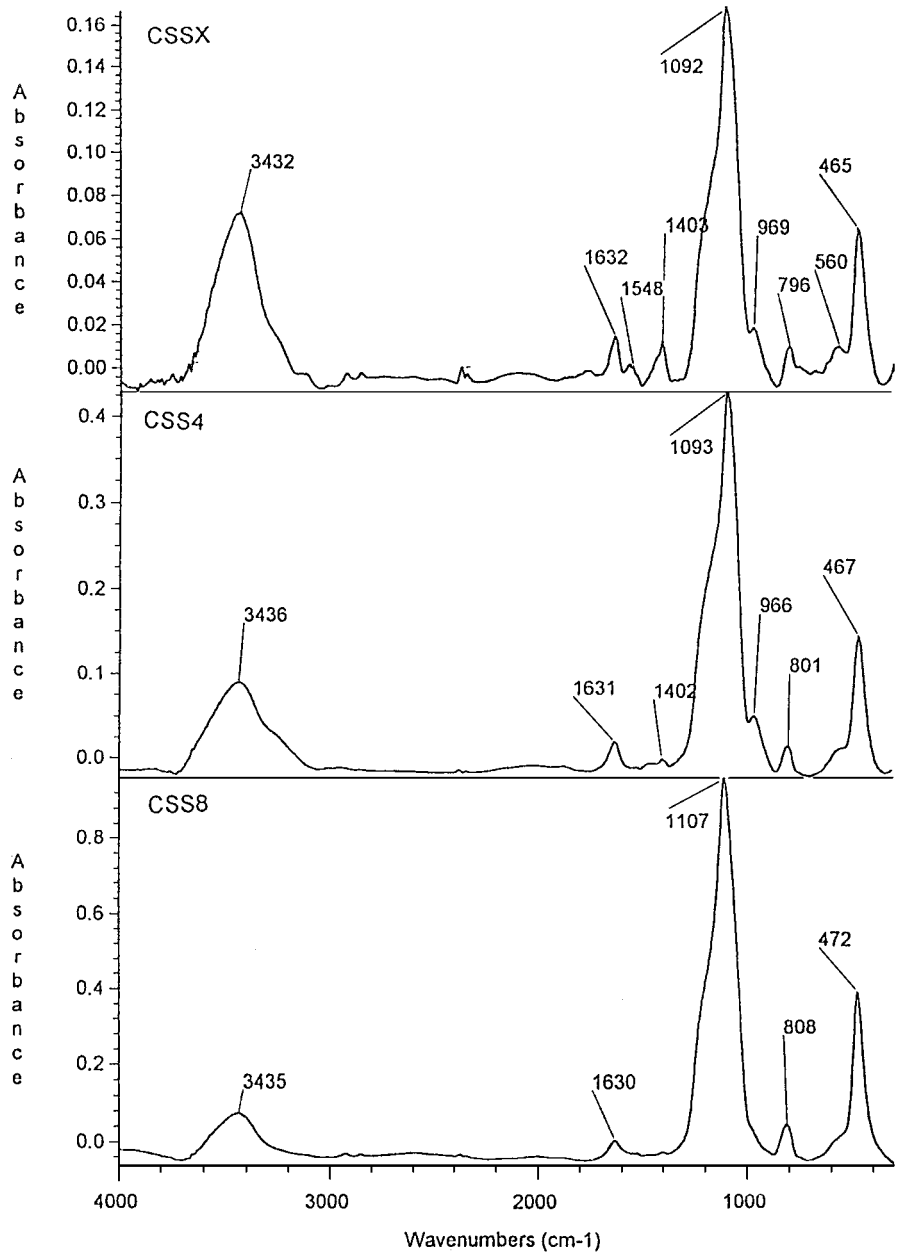

FIG. 1. Evolution of the solids as a function of thermal treatments. FTIR spectra of the xerogel (CSSX), the xerogel calcined at 673 K (CSS4), and the xerogel calcined at 1073 K (CSS8).

surface area of the calcined sample was even higher (by about 25%) than the surface area of the xerogel. The surface area of silica gels often increases when organic residuals (precursors and/or nonhydrolyzed alkoxides) are removed during calcination (11). On the other hand, a decrease in the surface area was observed as the calcination temperature increased up to 1073 K.

Fourier Transform Infrared Spectroscopy (FTIR)

The background infrared spectra of the xerogel (CSSX) and the catalysts calcined at 673 (CSS4) and 1073 K (CSS8), are displayed in Fig. 1. The spectra showed absorption bands at approximately 1100, 800, and 470 cm^{-1}, which are assigned to the different vibration modes of the Si–O bonds in the amorphous SiO_2. In the xerogel spectrum (CSSX), an absorption band at 1403 cm^{-1} is associated with vibrations of C–H bonds probably coming from residual organic compounds or incomplete hydrolysis of the alkoxides. The same holds for the absorption band at around 1540 cm^{-1} coming from the asymmetric stretching mode of vibration of the –COO bond (12a). These absorption bands decreased for the solid calcined at 673 K (CSS4) and practically

disappeared for the solid calcined at 1073 K (CSS8). The broad absorption band around 3450 cm^{-1} is due to the overlapping of the stretching mode of OH^- groups (11) and adsorbed water. Similarly, the band near 1630 cm^{-1} is associated with the bending mode of OH groups of molecularly adsorbed water (8). It must be emphasized that sample preparation, including that of the hygroscopic KBr, may largely contribute to these bands. Two bands are particularly sensitive to the thermal treatment of the sample, the one at 560 and the other at 960 cm^{-1} (stretching), associated with the presence of nonbonded oxygens $Si–O^-$ (12b). As the calcination temperature increased, shift of some of the absorption bands toward high frequencies and the disappearance of others (560 and 960 cm^{-1}) was observed, suggesting a rearrangement of the structure of the silica matrix.

The vibration of CuO bonds that appear at 575, 500, and 460 cm^{-1} (13) cannot be observed due to the presence of a broad band at 460 cm^{-1} from the support. In all spectra a shoulder around 600 cm^{-1} was observed and this could be an indication of Cu (II)–O species as reported in (8).

Temperature-Programmed Reduction (TPR)

The raw TPR profiles and the deconvoluted profiles of samples CSS4 and CSS8 are shown in Fig. 2. The sample calcined at 673 K began its reduction at a lower temperature than the catalyst calcined at 1073 K. The CSS4 sample showed a well defined peak with two contributions after this distinct feature. The reduction profile of sample CSS8 also showed three peaks but with a different distribution with respect to the CSS4 sample. The characteristic temperatures are summarized in Table 2. The hydrogen consumption indicates incomplete reduction of the copper oxide (Table 2). Encapsulation of copper is possible with the sol–gel preparation; therefore, the percentage of reduction may reflect this situation.

X-ray Photoelectron Spectroscopy (XPS)

The chemical state of the catalyst components and the relative concentration at the surface has been evaluated by XPS in both calcined and H_2-reduced samples. The binding energies (BE) of core electrons of the most abundant elements are compiled in Table 3. For the sake of clarity the Cu $2p_{3/2}$ core-level spectra of outgassed and H_2-reduced CSS4 and CSS8 samples are displayed in Fig. 3. From these spectra it is clear that the Cu $2p_{3/2}$ profile changed drastically upon reduction with hydrogen at 523 K. The calcined and outgassed samples showed the principal Cu $2p_{3/2}$ line somewhat above 933.4 eV with a shoulder on the high BE side, which is characteristic of Cu^{+2} species (14a–14c). The Cu^{+2} ions are also easily identified by the satellite peak, placed around 943 eV, whose origin is complex (15a–15d). Considering the asymmetry of the Cu $2p_{3/2}$ envelope, peaks of calcined and reduced samples have been deconvoluted into two contributions centered around 933.5 eV and somewhat above 934.6 eV. The disappearance of the satellite line and the simultaneous shift of the principal Cu $2p_{3/2}$ peak to lower BE upon H_2-reduction at 523 K, showed that after this treatment the copper species are reduced Cu^+ or Cu^0, but in no case is it Cu^{2+}. Judging from the shape and area of the Cu 2*p* satellites, some photoreduction of CuO phase might occur during the analysis of the outgassed samples and more specifically for sample CSS4 in which the intensity of the satellite is very small.

The surface atomic ratios Cu/Si, also summarized in Table 3, have been calculated from peak areas, normalized by photoelectron cross sections and mean free paths (16, 17). Cu/Si ratios are larger for the outgassed catalyst CSS4 and decreases by 37% upon reduction, suggesting aggregation of reduced copper species. Unexpectedly, the ratio Cu/Si was lower for sample CSS8 than for its CSS4 counterpart. This result, together with the dark color and a broad band around 350 nm in its diffuse reflectance spectrum, indicates that CuO clusters are developed in the calcined catalyst. Further sintering of copper species seems to occur in the reduced CSS8 sample, as evidenced by the decrease of the Cu/Si ratio in this sample.

TABLE 2

Characteristic Reduction Temperatures and Extent of Reduction of CuO–SiO_2 Sol–Gel Catalysts

Sample	Peak 1 T_{max} (K)	Peak 2 T_{max} (K)	Peak 3 T_{max} (K)	% Reduction
CSS4	520	610	705	94
CSS8	550	600	680	91

TABLE 3

Binding Energies, Auger Parameter, and Surface Atomic Ratios of Cu/SiO_2 Samples

Pretreatment	Si 2*p* (eV)	Cu $2p_{3/2}$ (eV)	α^A (eV)	Cu/Si at
CSS4, vac	103.4	934.0(74) 936.2(26)	—	0.0170
CSS4, H_2[a]	103.4	933.5(81) 934.9(19)	—	0.0103
CSS4, NO + H_2[b]	103.4	932.8(100)	1851.7 1848.7	0.0087
CSS8, vac	103.4	933.4(72) 935.6(28)	—	0.0105
CSS8, H_2[a]	103.4	933.1(76) 934.6(24)	—	0.0072
CSS8, NO + H_2[b]	103.4	932.8(100)	1851.4 1849.1	0.0064

Note. Values in parentheses are peak percentages.
[a] Reduction at 523 K for 1 h.
[b] Pretreatment at 723 K for 2 h.

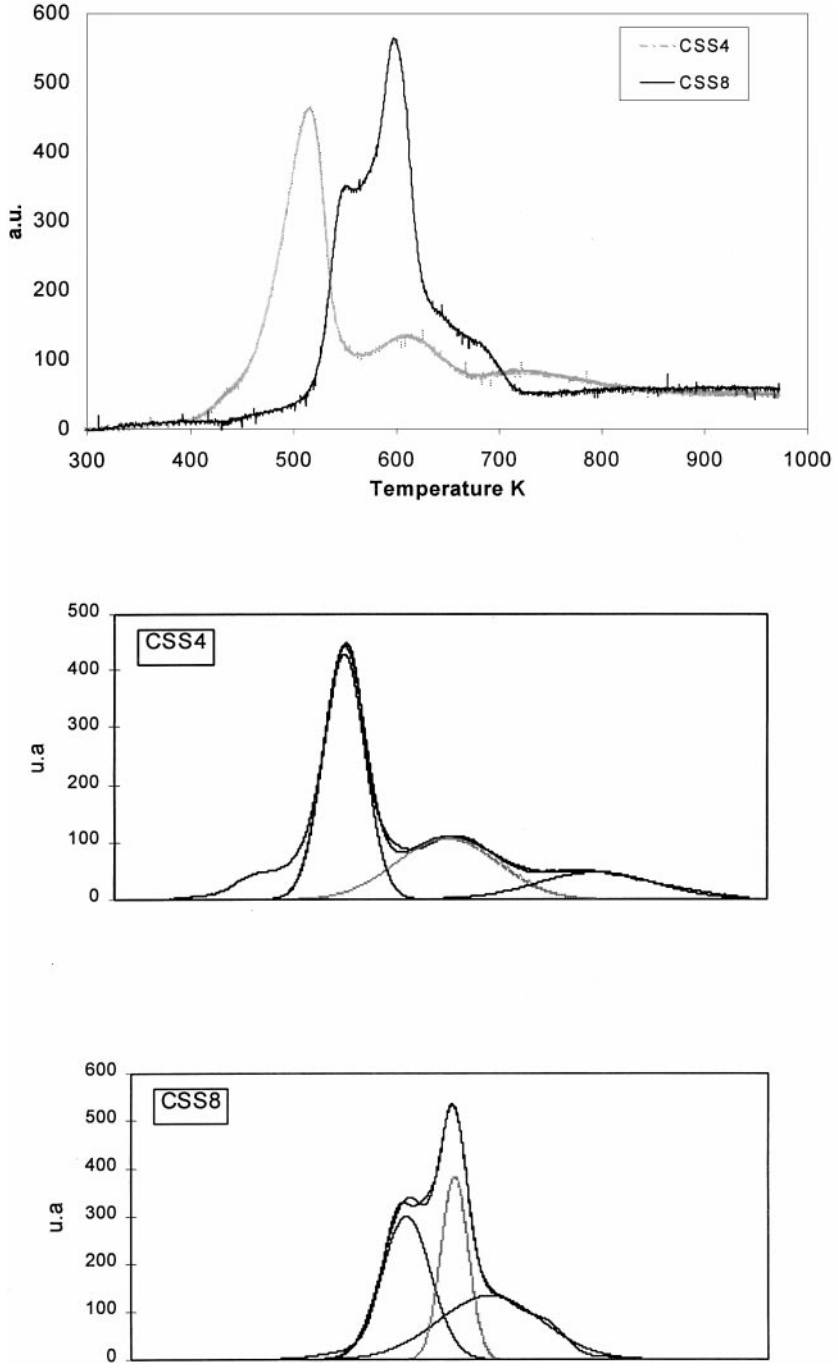

FIG. 2. Thermo-programmed reduction of samples calcined at 673 K (CSS4) and 1073 K (CSS8). Deconvoluted profiles.

In order to get an insight of the nature of copper species developed on the catalyst surface during on-stream operation, both CSS4 and CSS8 samples were pretreated under a $NO : H_2 = 1 : 1$ gas mixture at 723 K for 2 h within the pretreatment chamber of the XPS spectrometer and then analyzed. The BE of Cu $2p_{3/2}$ core level of both samples at 932.6–932.8 eV and the absence of satellite lines are conclusive evidence that copper became reduced (Cu^+ or Cu^0). Since the BE values of Cu^+ and Cu^0 are almost identical, the distinction between the Cu^+ and the Cu^0 species present on the catalyst surface is feasible only through examination of the Auger parameter (18a, 18b). The modified Auger parameter is defined by: $\alpha_A = h\nu + (Cu_{LMM} - Cu2p_{3/2})$, where α_A represents the difference between the kinetic energy of the Cu_{LMM} Auger electron and the Cu $2p_{3/2}$ photoelectron, and $h\nu$ is the energy of the incident photon. The observation

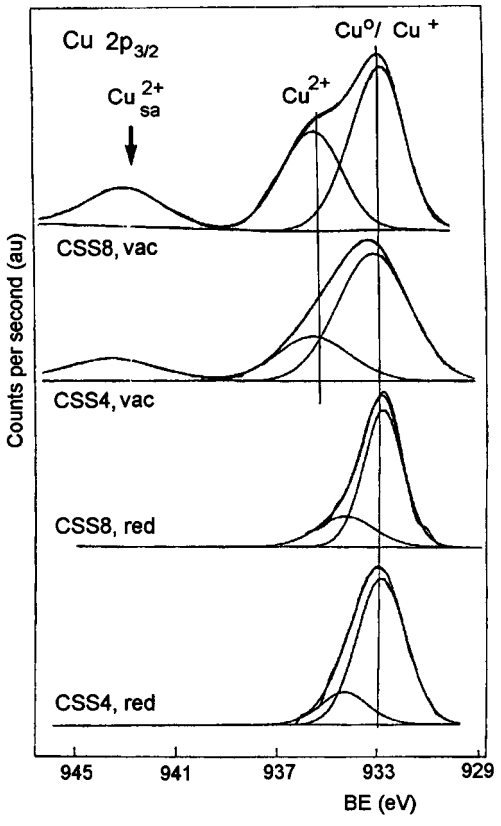

FIG. 3. Cu $2p_{3/2}$ core-level spectra of samples CSS4 and CSS8 subjected to outgassing and reduction treatments.

of two components for samples CSS4 and CSS8 (Table 3 and Fig. 4) allowed the conclusion that Cu^+ and Cu^0 species are simultaneously present on the surface of the catalysts exposed to the reactant mixture $NO + H_2$.

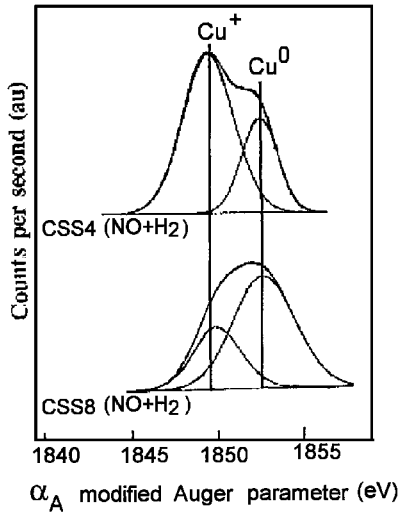

FIG. 4. Cu_{LMM} Auger parameter for samples CSS4 and CSS8 exposed to a $NO + H_2 = 1:1$ (molar ratio) at 723 K for 2 h within the pretreatment chamber of the spectrometer.

High-Resolution Electron Microscopy HRTEM

Results concerning the HREM characterization of the catalysts have been published elsewhere (19). Figure 5 shows low magnification electron micrographs of the calcined samples. From the images it is evident that the SiO_2 particles increased their size as the calcination temperature increased. The microstructure of the CSS4 catalyst, examined by high-resolution electron microscopy is shown in Fig. 6. Small crystallites in a structureless form can be observed on the surface of the amorphous silica. The mean size of these structures is 4 nm. A totally different picture is offered by the CSS8 sample (Fig. 7). In this case, apparently only the amorphous structure of the SiO_2 was observed. This would mean that the copper is either atomically dispersed or formed into clusters of such a size that they could not be detected by HRTEM. Another possibility is linked to the reaction of CuO and the support when heating under oxidizing atmospheres, leading to the formation of a structureless or amorphous silicate compound.

The microstructure characterization of the catalysts after reaction ($NO + H_2$, $NO/H_2 = 0.5$, 373–873 K) showed different evolution. Figure 8 shows a typical image of the catalyst calcined at 673 K after a catalytic run. Crystallites with well-defined structures are evident. The mean particle size is in the range of 10–20 nm. Figure 9 shows an image of the CSS8 catalyst after reaction. Segregation of small crystals on the edges of the silica support were identified. The mean size of these crystallites is in the range 7–9 nm. HRTEM images showed that copper oxide changes its morphology and crystal structure, depending on the treatment that the catalyst has undergone (calcination and redox treatments during reaction).

The HRTEM images were digitized and Fourier transform patterns were obtained in order to measure with relatively good precision the interplanar distances in particles and to make the phase assignment. The results are shown in Table 4 where the color of the sample at each stage of the analysis has been included. Measurements showed that in the CSS4 sample, copper is present as CuO crystallites in a structureless form. Furthermore, this sample has the blue-green color characteristic of the presence of cupric ions Cu^{+2} incorporated into silica (20). This suggests that besides the small crystallites, copper oxide is either highly dispersed or forms clusters of such a size that could not be detected. Under a "reducing atmosphere," i.e., under stream, the sample first showed a reddish-purple color which changed to dark gray after few minutes of exposure to air. This result is interpreted as a change of valence state from a mixed ($Cu^0 + Cu^{1+}$) valence to a main valence of copper Cu^{2+}. Finally, the main crystalline form observed corresponds to CuO (Table 4).

For sample CSS8 no traces of crystalline copper were detected. After reaction, segregation of crystallites to the borders of the silica particles was shown, demonstrating the influence of the redox treatments (catalytic reaction)

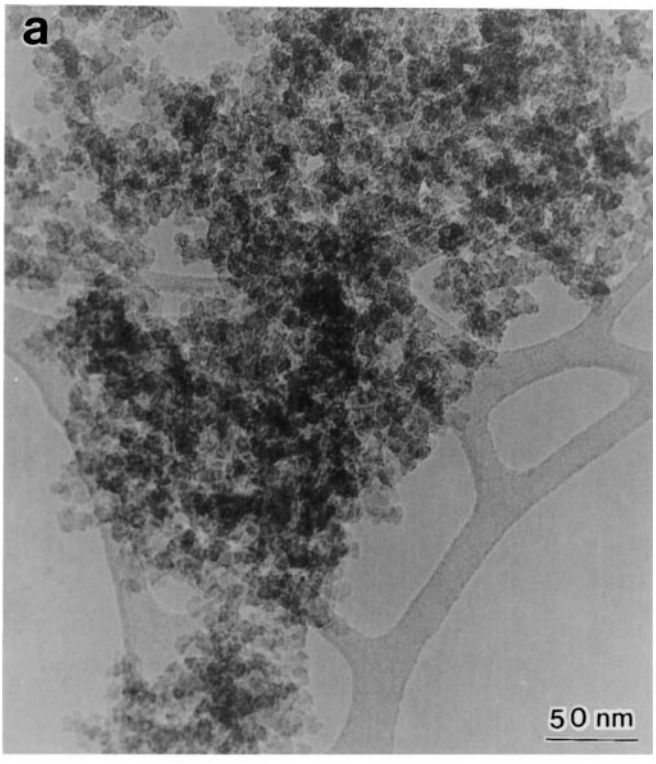

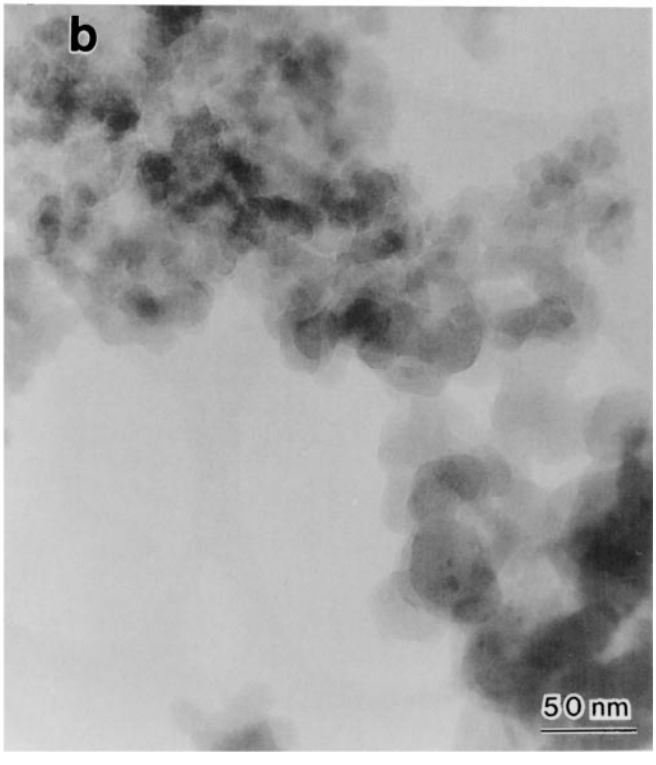

FIG. 5. Low magnification micrographs of samples calcined at (a) 673 (CSS4) and (b) 1073 K (CSS8). (Reprinted from (19) M. Benaissa and G. Diaz, *Microsc. Res. Tech.* **40**, 49 (1998). Copyright © 1998 Wiley–Liss. Reprinted by permission of Wiley–Liss, Inc., a subsidiary of John Wiley & Sons, Inc.)

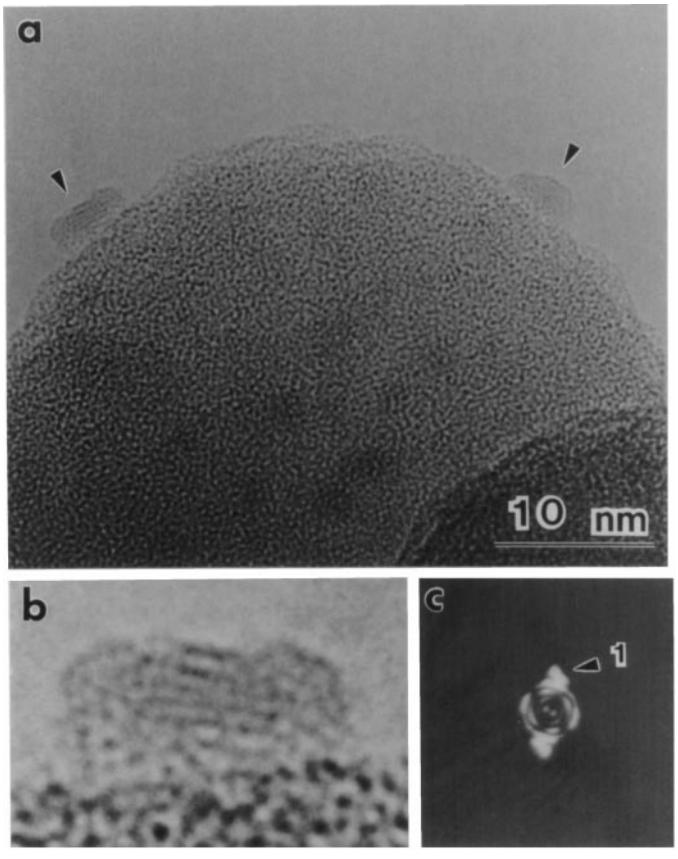

FIG. 6. (a) HRTEM micrographs of CSS4 catalyst. Supported small CuO crystallites are indicated by arrowheads. (b) High magnified CuO crystallite and (c) its corresponding FFT. (Reprinted from (19) M. Benaissa and G. Diaz, *Microsc. Res. Tech.* **40**, 49 (1998). Copyright © 1998 Wiley–Liss. Reprinted by permission of Wiley–Liss, Inc., a subsidiary of John Wiley & Sons, Inc.)

on incorporated copper ions. This result suggests that these incorporated ions enhance in "reducing atmospheres" the ready formation of such crystallites. This phenomenon is also thought to occur in the CSS4 sample, which explains the

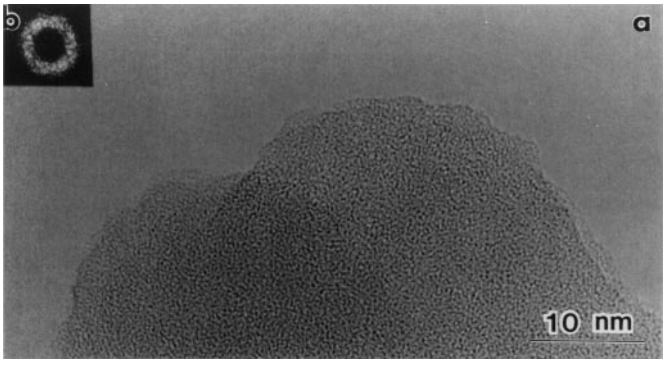

FIG. 7. (a) Typical HRTEM micrograph of CSS8 catalyst. (b) At the inset FFT. (Reprinted from (19) M. Benaissa and G. Diaz, *Microsc. Res. Tech.* **40**, 49 (1998). Copyright © 1998 Wiley–Liss. Reprinted by permission of Wiley–Liss, Inc., a subsidiary of John Wiley & Sons, Inc.)

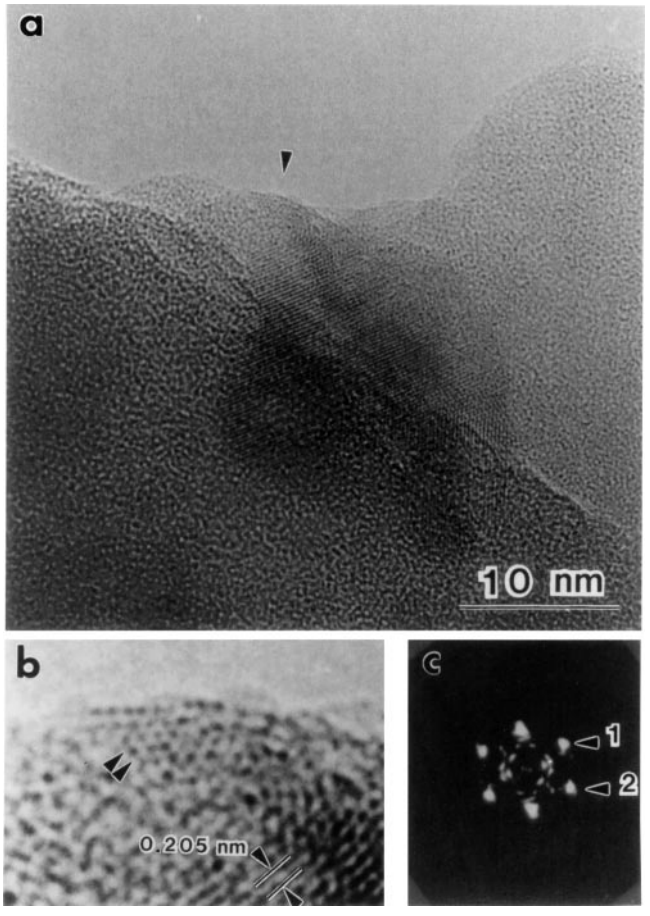

FIG. 8. (a) HRTEM micrograph of CSS4 catalyst after reaction. ($NO + H_2$, $T = 298$–973 K). A crystallite is shown by the arrowhead. (b) Highly magnified image of this area. (c) FFT corresponding to the top part (indicated by double arrowhead) of the image shown in (b). (Reprinted from (19) M. Benaissa and G. Diaz, *Microsc. Res. Tech.* **40**, 49 (1998). Copyright © 1998 Wiley–Liss. Reprinted by permission of Wiley–Liss, Inc., a subsidiary of John Wiley & Sons, Inc.)

TABLE 4

Estimated Phases Determined by HREM in Calcined Samples and after Reaction

Catalyst	d_{exp} (nm) ($\Delta = \pm 0.005$ nm)	ϕ (nm)	Phase	Sample color
CSS4	Reflect. 1: 0.357	4	CuO	Blue-green
CSS4R	Reflect. 1: 0.205	10–20	$Cu + CuO_x$	Reddish purple
	Reflect. 2: 0.191		↓ air ↓	↓
			$Cu + CuO$	Dark gray[a]
CSS8	—	—	Glassy	Dark gray
CSS8R	0.202	7–9	$Cu + Cu_2O$	Reddish purple

Note. CSS4R, CSS8R, samples after reaction ($NO + H_2$, $NO/H_2 = 0.5$, 298–873 K). Reflect. 1, and 2; reflections in FFT.

[a] HREM analyzed.

size of the crystallites; i.e., in addition to the spread of the deposited crystallites, incorporated copper ions segregate to the surface and migrate to join the deposited outside crystallites. The segregated crystals in sample CSS8 were identified as a mixture of Cu^0 and Cu_2O along with some areas showing structural defects (Fig. 9). These small areas are thought to correspond to defective Cu_2O structures. A defect structure of Cu_2O, which corresponds to $CuO_{0.67}(Cu_3O_2)$, is well accepted to occur either in thin films (21) or in small particles (22) as an intermediate and suggests that the observed defects may correspond to a stable copper (I) oxide defect structure.

Catalytic Activity ($NO + H_2$)

(a) Calcined samples. The overall activity of CSS4 and CSS8 catalysts for NO reduction by hydrogen at a molar ratio $NO/H_2 = 0.5$ is shown in Fig. 10. At these experimental

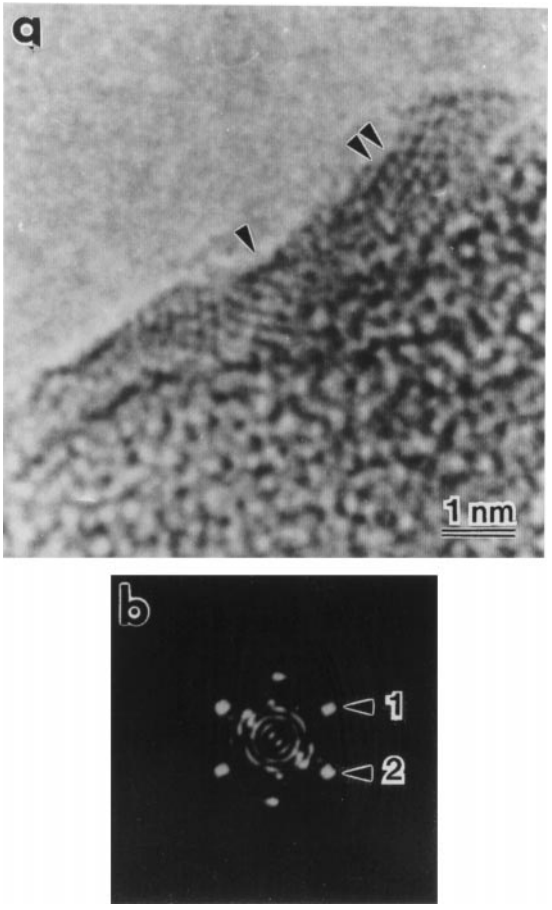

FIG. 9. (a) A typical HRTEM micrograph of CSS8 catalyst after reaction ($NO + H_2$, $T = 298$–973 K). A segregation of copper phase is observed. (b) FFT of the top right part of the crystallite (indicated by double arrowhead in (a)). A small area showing structural defects is indicated by the single arrowhead in (a). (Reprinted from (19) M. Benaissa and G. Diaz, *Microsc. Res. Tech.* **40**, 49 (1998). Copyright © 1998 Wiley–Liss. Reprinted by permission of Wiley–Liss, Inc., a subsidiary of John Wiley & Sons, Inc.)

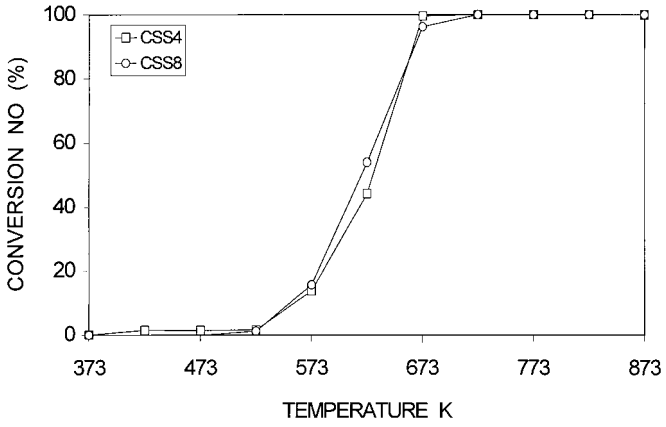

FIG. 10. Overall activity as a function of reaction temperature ($NO + H_2$, $NO/H_2 = 0.5$) of CSS4 and CSS8 catalysts.

conditions only slight differences were observed for the NO conversion between CSS4 and CSS8 catalysts. Total conversion of NO is achieved at 723 K in both samples. When a molar ratio $NO/H_2 = 1$ was used, the total activity of the samples decreased and more pronounced differences in reactivity between samples were observed (Fig. 11). The catalyst calcined at 1073 K is more active than the catalyst calcined at lower temperature, as can be observed from data in Table 5 where the light-off temperature (T_e), the temperature for 50% conversion of NO (T_{50}), and the conversion at 873 K are presented. The dispersion of the copper phase calculated from dissociative N_2O adsorption, the turnover frequencies (TOF), and the apparent activation energies calculated in the low conversion region (up to 623 K) are compiled in Table 6. Catalyst CSS8 showed a moderately higher dispersion than CSS4 sample. The apparent activation energy for these catalysts in the range 548–623 K is 11 and 13 kcal/mol for CSS8 and CSS4 catalysts, respectively. Finally, the TOF calculated at 623 K is 2.5 times higher for CSS8 catalyst than for the CSS4 sample.

TABLE 5

Reactivity of CuO–SiO_2 Samples: $NO + H_2$, $NO/H_2 = 1$

Catalyst	T_e (K)	T_{50} (K)	χ_{873} (%)
CSS4	623	788	77
CSS8	573	708	76

Note. χ_{873} (%), conversion of NO at 873 K.

(b) Reduced samples. The reactivity of prereduced samples was also investigated. For this purpose calcined samples were subjected to a temperature programmed reduction from 298 to 673 K prior to the catalytic run ($NO/H_2 = 0.5$). The notation for samples will be RCSS4 and RCSS8 for CSS4 and CSS8 catalysts, respectively. Figure 12 shows the behavior of the RCSS4 catalyst. Prereduction of the CSS4 sample led to an increase of activity at low temperatures (<573 K) and a decrease of activity at higher temperatures. On the contrary, the same pretreatment performed in the CSS8 catalyst did not have a major influence in the catalytic behavior of the sample; RCSS8 catalyst is slightly more active at low temperatures and slightly less active at higher temperatures compared to the calcined sample (Fig. 13). At equimolar NO/H_2 ratio (not presented), RCSS4 catalyst showed a substantially lower activity in the whole range of temperature compared to the calcined sample. For RCSS8 catalyst, a decrease in activity was also observed (~15% in the worst case).

(c) Time on-stream. Time on stream experiments were performed in order to estimate the stability of these

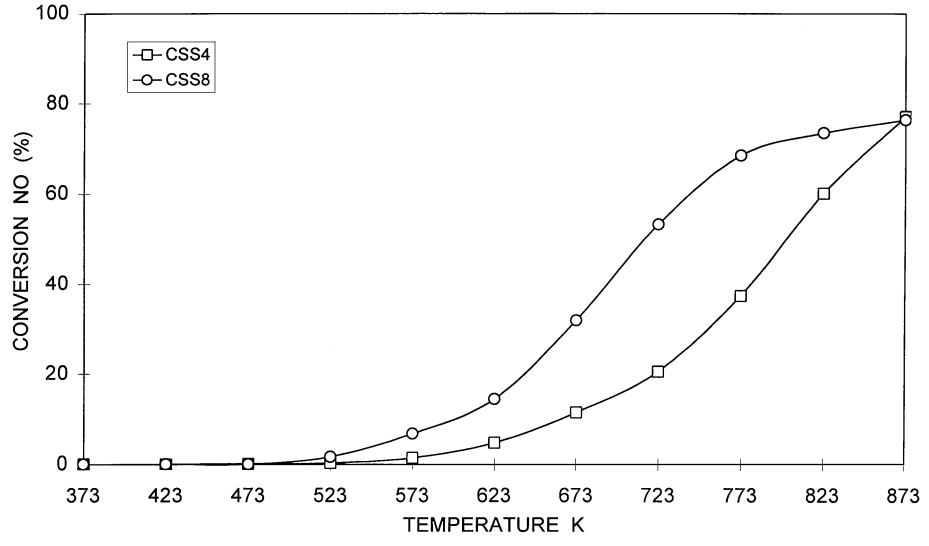

FIG. 11. Overall activity as a function of reaction temperature ($NO + H_2$, $NO/H_2 = 1$) of CSS4 and CSS8 catalysts.

TABLE 6

Dispersion, Turnover Frequencies, and Apparent Activation Energies $CuO–SiO_2$ Catalysts, $NO + H_2$, $NO/H_2 = 1$

Catalyst	Dispersion[a] (%)	TOF × 10^2 [b] (s^{-1})	E_a[c] (K_{cal}/mol)
CSS4	23	0.72	13
CSS8	32	1.83	11

[a] Calculated from dissociative N_2O adsorption.
[b] TOF for NO reaction calculated at 623 K.
[c] Determined in the 548–623 K range.

sol–gel catalysts ($NO/H_2 = 0.5$, $T = 673$ K). Figure 14 shows the behavior of the CSS4 and CSS8 catalysts compared to samples prepared by the classical impregnation method and identified as CSI4 and CSI8 (same copper precursor, same CuO nominal content, and similar calcination procedures were used for these preparations). Differences are observed, the catalysts prepared by conventional methods had lost about 50% of their ability to convert the NO after 6 h of time on-stream. On the contrary, sol–gel catalysts were very stable. This behavior was also observed in the case of an equimolar NO/H_2 ratio. The sample calcined at 673 K apparently showed an induction period. The activity increased in more than 1 h to reach a stable value that lasted for the entire run.

(d) Selectivity. The products for the $NO + H_2$ reaction are N_2, N_2O, NH_3, and H_2O. At a $NO/H_2 = 1$ molar ratio, the selectivity plotted as ($N_2 + N_2O$) (mol%) is shown in Fig. 15. The ($N_2 + N_2O$) concentration is around 70 mol% at 873 K. The curve followed nearly the same trend as that of the overall activity. Ammonia was not detected at significant levels under this experimental condition, but the slight decrease in ($N_2 + N_2O$) concentration at the end of the run is related to the presence of this compound. At higher H_2 concentration ($NO/H_2 = 0.5$) ammonia concentration became important.

4. DISCUSSION

The most significant features of these $CuO–SiO_2$ sol–gel catalysts evidenced by the various characterization techniques may be summarized as follows: (i) Different species are present in the catalysts as a function of the calcination temperature; i.e., the sample calcined at 1073 K had copper species that reduced at a higher temperature than those present in the sample calcined at 673 K. (ii) Small crystallites identified as CuO were observed in the sample calcined at 673 K. On the contrary, no CuO structure was observed in the catalyst calcined at 1073 K. After the reaction, sintering was observed in both catalysts but the extent of this phenomenon was different for each sample. A mixture of reduced and oxidized phases (in the sample calcined at 673 K) and reduced phases (in the sample calcined at 1073 K) was determined after reaction. (iii) Catalyst reduction at 523 K led to the disappearance of satellite line and the simultaneous shift of the principal Cu $2p_{3/2}$ peak to lower BE. Both facts are conclusive that copper species were reduced Cu^+ or Cu^0, but in no case was it Cu^{2+}. The surface atomic ratios Cu/Si were larger for the outgassed CSS4 catalyst and markedly decreased upon H_2-reduction, suggesting aggregation of reduced copper species. The Cu/Si ratio is even lower for sample CSS8 than for its CSS4 counterpart, indicating that CuO clusters are developed in the calcined catalyst. Further sintering occurs upon H_2 reduction. (iv) Dissociative N_2O adsorption showed a moderately higher dispersion of the copper phase in CSS8 catalyst. Reactivity differences in the $NO + H_2$ reaction were observed for calcined and prereduced samples as a function of the

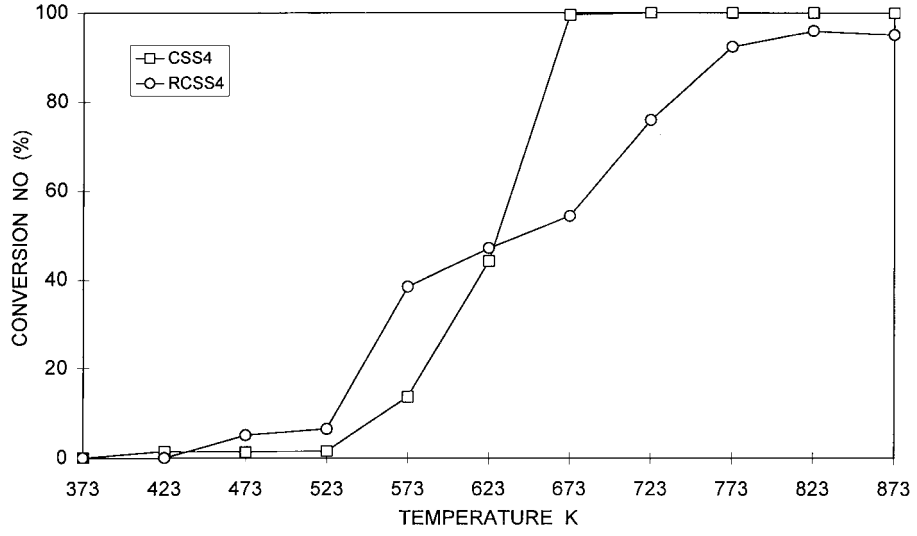

FIG. 12. Catalytic activity of calcined (CSS4) and prereduced (RCSS4) catalyst ($NO + H_2$, $NO/H_2 = 0.5$).

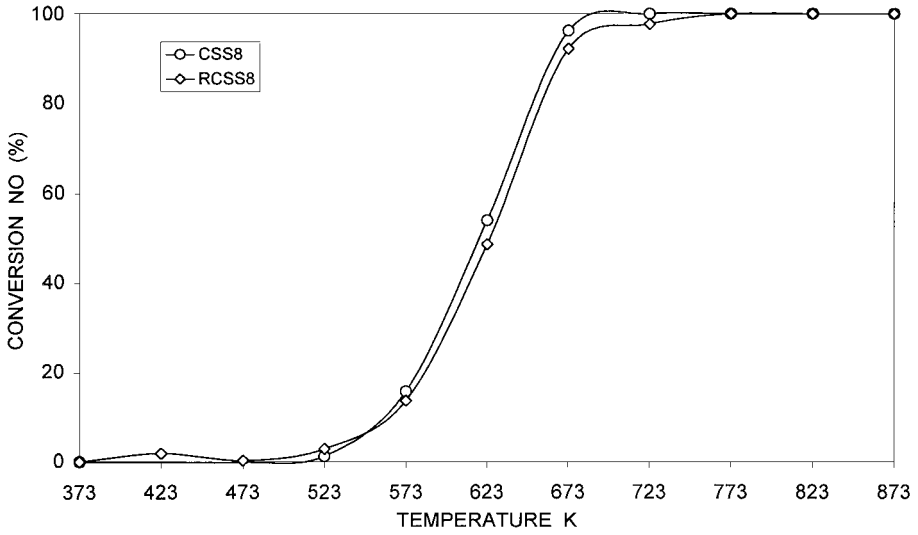

FIG. 13. Catalytic activity of calcined (CSS8) and prereduced (RCSS8) catalyst ($NO + H_2$, $NO/H_2 = 0.5$).

calcination temperature. At a $NO/H_2 = 1$ molar ratio, the calculated TOF was 2.5 times higher for a catalyst calcined at higher temperature. Remarkable stability of both sol–gel catalysts was observed compared to samples prepared by conventional methods.

From all these results it seems clear that the preparation method on the one hand and the calcination temperature of the catalysts on the other are relevant to the microstructure and catalytic behavior of the samples.

The microstructure of the calcined catalysts (small CuO crystals along with a vitreous structure in sample CSS4 and only an amorphous structure in sample CSS8) may be correlated with the reduction properties of the samples. The effect of dispersion of CuO in the reduction of the phase has been documented. Bond *et al.* (23) in a study of the influence of the support on the reduction properties of copper based catalysts, mentioned that two kinds of copper species are present in silica and alumina catalysts: CuO particles which reduce in a very narrow temperature range and dispersed Cu(II) species which reduce at high temperatures. Gentry and Walsh (24), on the other hand, showed that copper oxide supported on silica presented two copper species, dispersed CuO and copper silicate. TPR profiles showed that the first one reduces at lower temperatures than the second one and that the reduction temperature of the species in strong interaction with the support depends on the calcination temperature. Guerreiro *et al.* (25), studying copper on silica catalysts prepared by ionic exchange, report the

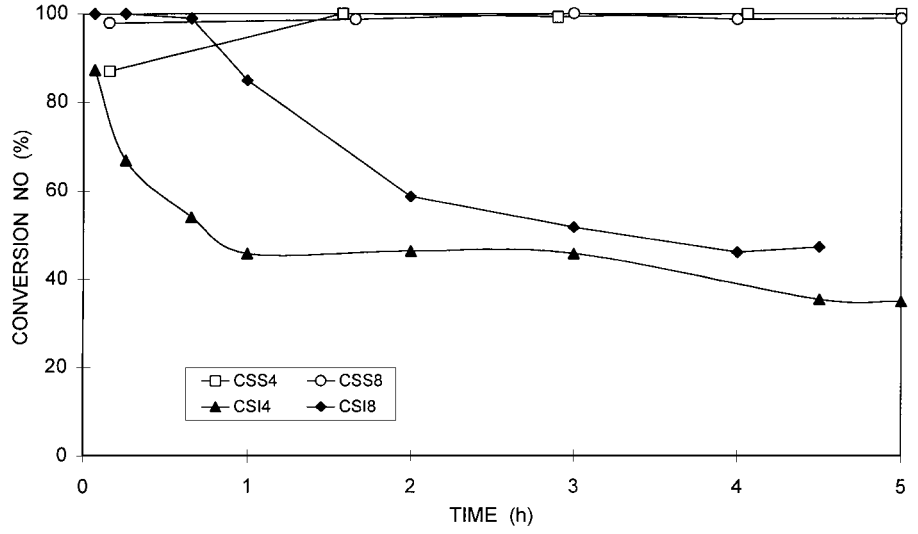

FIG. 14. Time on-stream experiment showing the behavior of CSS4 and CSS8 sol–gel catalysts along with CSI4 and CSI8 impregnated samples.

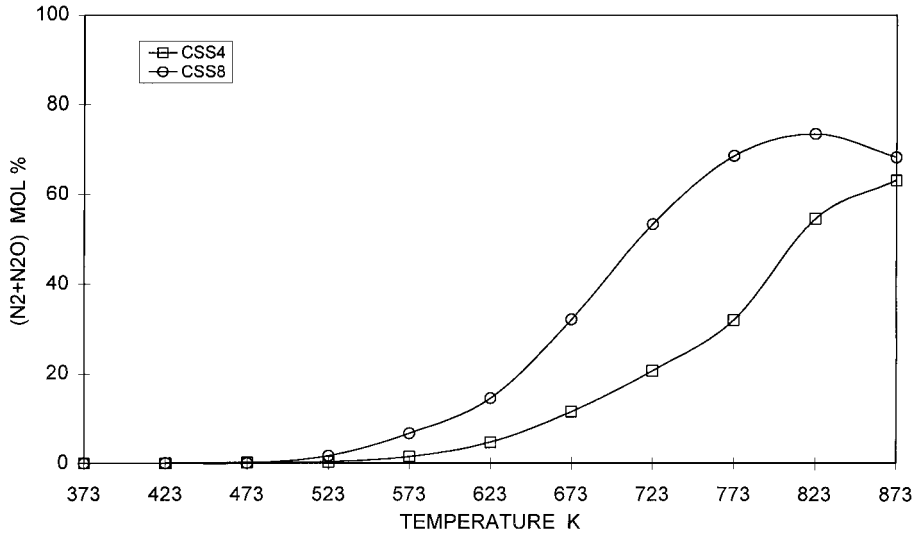

FIG. 15. Selectivity for ($N_2 + N_2O$) in mol% as a function of the reaction temperature ($NO + H_2$, $NO/H_2 = 1$).

presence of two reduction peaks in TPR studies. The maxima of these peaks are between 523 and 623 K and 873 and 923 K, respectively. Deconvolution of the first one showed two contributions. The first is the one-step reduction of low interacted copper species ($Cu^{+2} \rightarrow Cu^0$) and the second is the partial reduction of highly dispersed and surface interacted species ($Cu^{+2} \rightarrow Cu^{+1}$). The second peak is related to the second step reduction of this species ($Cu^{+1} \rightarrow Cu^0$).

The TPR profiles of the sol–gel catalysts in this work may be correlated with the occurrence of low- and high-interacted copper species as a function of the calcination temperature. Reduction at lower temperature could be related to the presence of small CuO crystallites as shown by the HRTEM characterization; reduction at higher temperatures could be related to copper species not detected by HRTEM. These copper species may be visualized as "stabilized" species resulting from the preparation method. UV–VIS–NIR characterization of samples prepared by the same experimental procedure pointed out the existence of two copper (II) species in the samples, one within the silica network and the other one as highly dispersed clusters (8).

Dispersion of the copper phase calculated from dissociative N_2O adsorption followed the same trend suggested by the HREM examination of the catalysts (a better dispersion for CSS8 than for CSS4 catalyst). XPS measurements showed, on the contrary, that CSS4 catalyst was better dispersed. This apparent disagreement may have its origin in the fact that XPS is a sensitive-surface technique (0–3 nm), while chemisorption is related to the entire surface of the solid.

The occurrence of species of different nature (low and high interacted species) was evidenced when the catalytic behavior of the calcined and prereduced samples was studied. The reactive surface that is generated upon reduction of the calcined sample and its evolution during the reaction seem to be different for each sample. The nature of the active site and the mechanism associated to both the decomposition and the reduction of NO in Cu-based catalysts has been a matter of controversy. Copper species with various oxidation states (Cu^0, Cu^{1+}, Cu^{2+}) have been invoked to participate in the reaction mechanism (26). In the presence of a reductant (e.g., H_2 or CO), this transforms copper ions in a reduced copper site; the dissociative adsorption of NO produces N_2 and oxygen atoms adsorbed on the surface. The reductant regenerates the active site by removing the adsorbed oxygen atoms (27). In Cu–ZSM-5 catalysts, the rate of NO decomposition has been related to the cuprous ion concentration (28).

According to this model, the prereduction of CSS4 sample led, as expected, to an increase of catalytic activity compared to that seen in the calcined sample. Furthermore, the behavior of the catalysts as a function of the hydrogen concentration is also an indication of the role of the reductant in the reaction mechanism (27). Nevertheless, for this sample, a decrease of activity at higher temperatures was also observed. The explanation for this decay in activity can be related to a loss of active surface area due to sintering. For the CSS4 catalyst, the HRTEM showed an increase in particle size after reaction (Fig. 8). This fact could be an indication of the evolution of the active phase when subjected to thermal treatments as the catalytic reaction. The prereduction of the sample and the reaction itself could, therefore, have an important effect on the evolution of the surface of the small (CuO and/or Cu) crystallites present in the sample.

For the sample calcined at 1073 K, the prereduction of the catalyst had no major effect in the activity of the sample. HRTEM examination of the CSS8 sample after reaction

showed, on the other hand, a lower sintering of the copper phase compared to that seen in CSS4, which agrees with the Cu/Si ratios derived from XPS. The behavior of the CSS8 catalyst cannot then be related only to a sintering phenomenon, and it seems that the reactive surface that is generated *in situ* during reaction in the calcined sample is not very different from that generated in a prereduced sample. This could mean that copper species at the surface of both catalysts (calcined and reduced) undergo similar processes (redox and sintering) and this as a consequence of the original microstructure of the catalyst.

Both samples prepared by the sol–gel method showed remarkable stability in time on-stream when compared to the catalysts prepared by impregnation. The sol–gel method offers the possibility of stabilizing ions or structures of ions in the oxide network (6). In our case this fact is clearly shown by the catalytic activity of the CSS4 and CSS8 samples after 6 h on stream; i.e., the active phase in these catalysts is more stable toward sintering than in catalysts prepared by a classical method. In catalysts prepared by conventional methods, a severe loss of the active surface could easily explain their behavior. It is known from the literature that the mobility of metallic copper in catalysts prepared by impregnation leads to significant sintering when reduction treatments are performed at 573 K (29). Indeed, HREM examination of calcined catalysts prepared by impregnation showed already the presence of CuO crystallites with a particle size higher than 15.0 nm. Particles of this size were never observed in the catalysts prepared by the sol–gel method. On the other hand, no clear interpretation can be given for the presence of an induction period in catalyst CSS4.

We can speculate that dispersed copper species stabilized by the support, as a consequence of the preparation method, are responsible for the catalytic behavior of the samples when compared to catalysts prepared by conventional methods such as impregnation. As an alternative, the possibility of formation of a silicate compound from reaction of the CuO with the support in catalyst calcined at high temperature has been mentioned before; nevertheless, the characterization techniques used in this work do not provide evidence of the presence of such a phase.

Kohler *et al.* (22) suggested that the low deactivation rate for Cu/SiO_2 prepared by ion-exchange is related to a strong interaction between small copper particles and the ion exchanged Cu(I) present on the silica surface. On the other hand, stabilization of Cu^{+1} species by the support has been mentioned to be required for the NO decomposition on model Cu/Al_2O_3 (0001) catalysts (30).

Copper species with various aggregation states may coexist at the surface of the sol–gel catalysts. Some of these species are stabilized by the support. The dispersion measurements showed only moderate differences between both catalysts. The redox behavior of these surface species will be different and therefore, various oxidation states of copper will be available during reaction. The strength of the adsorption bond of the NO depends on the copper oxidation state; thus, the ability of these species to activate the NO will be a function of their aggregation state and stability under reaction. The equilibrium between $Cu^0/Cu^{1+}/Cu^{2+}$ species and their occurrence during reaction, influenced by the interaction with the support and the concentration of the reductant, will determine the behavior of the catalyst. Supporting this, the Auger parameter determined on catalysts after reaction showed that the relative abundance of reduced Cu^0/Cu^{1+} species, present on the surface of the catalysts, is different in each sample (Fig. 4). Stabilization of active species through the support due to the preparation method and to the calcination treatments has important implications on the activity of the catalyst and the resistance of the active phase toward sintering.

CONCLUDING REMARKS

In the present study, CuO–SiO_2 catalysts prepared by sol–gel and calcined at 673 and 1073 K were characterized by BET, FTIR, TPR, dissociative N_2O adsorption, XPS, HRTEM techniques, and the reactivity of the samples was evaluated in the NO reduction by hydrogen in the 373–873 K range. The following conclusions can be drawn: (i) FTIR shows the typical absorption bands corresponding to the vibration modes of the SiO_2. The surface area of the solids decreases as the calcination temperature increases. (ii) The preparation method and the calcination temperature are relevant to the microstructure of the solids in such a way that stabilization of dispersed copper species not detected by HRTEM is achieved for samples calcined at high temperature along with small CuO crystallites in samples calcined at low temperature. The occurrence of these stabilized species are thought to be related to the reduction properties of the copper phase in the samples. Dissociative N_2O adsorption shows a moderately better dispersion for catalyst calcined at high temperature. (iii) Reduced catalysts show after reduction treatments not only a disappearance of satellite line but also a shift of the principal Cu $2p_{3/2}$ peak to lower BE. Both facts are conclusive that Cu^{+2} species became reduced to Cu^+ and Cu^0. Measurements of the Cu_{LMM} line in catalysts exposed to the $NO + H_2$ mixture allow the conclusion that Cu^+ and Cu^0 are simultaneously present on the surface of the catalysts exposed to the reactant mixture $NO + H_2$. In addition, the relative contribution of each reduced species on the surface of the catalyst is different. The Cu/Si ratio in the samples decreases upon H_2 reduction, indicating sintering of copper species. (iv) The catalysts were active for NO reduction by hydrogen. Remarkable stability of the sol–gel catalysts in time on-stream was observed compared to catalysts prepared by conventional methods (impregnation). (v) The observed differences could be an indication of the various properties of the Cu species while

being in or out the support framework after the calcination process.

ACKNOWLEDGMENTS

Thanks to Dr. Margarita Viniegra and Dr. Sergio Fuentes for stimulating discussions, to Dr. José Saniger for making available to us the FTIR spectrometer, to Mr. Alfredo Sánchez for the prints, and to CONACYT for funding.

REFERENCES

1. Taylor, K. C., *Catal. Rev. Sci. Eng.* **35**(4), 457 (1993).
2. (a) Iwamoto, M., and Hamada, H., *Catal. Today* **17**, 94 (1991); (b) Iwamoto, M., *Stud. Surf. Sci. Catal.* **54**, 121 (1990).
3. Shimokawage, M., Takezawa, N., and Kobayashi, H., *Appl. Catal.* **2**, 379 (1982).
4. De Jong, K. P., Geus, J. W., and Joziasse, *J. Appl. Surf. Sci.* **6**, 273 (1980).
5. van der Grift, C. J. G., Willers, A. F., Joghi, B. P. J., van Beijimen, J., de Boer, M., Versluijs-Helder, M., and Geus, J. W., *J. Catal.* **131**, 178 (1991).
6. (a) Yan, J., Buckley, A. M., and Greenblatt, M., *J. Non Cryst. Solids* **180**, 180 (1995); (b) Gracinda Ferreira da Silva, M., and Fernandez Navarro, J. M., *J. Non-Cryst. Solids* **100**, 447 (1988).
7. Buckley, A. M., and Greenblatt, M., *J. Non-Cryst. Solids* **146**, 97 (1992).
8. Cordoba, G., Arroyo, R., Fierro, J. L. G., and Viniegra, M., *J. Solid State Chem*. **123**, 93 (1996).
9. Fierro, G., Lo Jocano, M., Inversi, M., Porta, P., Lavecchia, R., and Cioci, F. L., *J. Catal.* **148**, 709 (1994).
10. Briggs, D., and Seah, M. P. (Eds.), "Practical Surface Analysis: Auger and X-ray Photoelectron Spectroscopy" 2nd ed. Wiley, Chichester, 1990.
11. Yamane, M., Aso, S., Okano, S., and Sakaino, T., *J. Mater. Sci.* **14**, 607 (1979).
12. (a) Guglielminoti, E. W., *Langmuir* **6**, 1455 (1990); (b) Decontignies, M., Phalippou, J., and Zarzycki, J., *J. Mater. Sci.* **13**, 2605 (1978).
13. Orel, B., Svegel, F., Bukovec, N., and Kosec, M., *Bull. Soc. Chim. Fr.* 122 (1963).
14. (a) Hermann, R. G., Klier, K., Simmons, G. W., Finn, P. B., Bulko, J. B., and Kobylinski, T. P., *J. Catal.* **56**, 407 (1979); (b) Okamoto, Y., Fukino, K., Imanaka, T., and Teranishi, S., *J. Phys. Chem*. **87**, 3740 (1983); (c) Garbassi, F., and Petrini, G., *J. Catal.* **90**, 113 (1984).
15. (a) Kim, K. S., *J. Electron Spectrosc. Relat. Phenom*. **3**, 217 (1974); (b) van der Laan, G., Westra, C., Hass, C., and Sawatzky, G. A., *Phys. Rev. B* **23**, 4369 (1981); (c) Okada, K., and Kotani, A., *J. Electron Spectrosc. Relat. Phenom*. **86**, 119 (1997); (d) Parmigiani, F., and Sangaletti, L., *J. Electron Spectrosc. Relat. Phenom*. **66**, 223 (1994).
16. Scofield, J. H., *J. Electron Spectrosc. Relat. Phenom*. **8**, 129 (1976).
17. Penn, D. R., *J. Electron Spectrosc. Relat. Phenom*. **9**, 29 (1976).
18. (a) Fierro, J. L. G., *Catal. Rev.-Sci. Eng.* **34**, 255 (1993); (b) Tavares Figuereido, R., Martinez-Arias, A., Lopez Granados, M., and Fierro, J. L. G., *J. Catal.* **178**, 146 (1998).
19. Benaissa, M., and Diaz, G., *Microsc. Res. Tech.* **40**, 49 (1998).
20. Bae, B. S., and Weinberg, M. V., *J. Non-Cryst. Solids* **168**, 223 (1994).
21. Wieder, H., and Czanderna, A. W., *J. Phys. Chem*. **66**, 816 (1962); Yanase, A., and Komiyama, H., *Surf. Sci.* **248**, 11 (1991).
22. Kohler, M. A., Curry-Hyde, H. E., Hughes, A. E., Sexton, B. A., and Cant, N. W., *J. Catal.* **108**, 323 (1987).
23. Bond, G. C., Namijo, S. N., and Wakema, J. S., *J. Mol. Catal.* **64**, 305 (1991).
24. Gentry, S. J., and Walsh, P. T., *J. Chem. Soc. Faraday Trans. I* **78**, 1515 (1982).
25. Guerreiro, E. D., Gorriz, O. F., Rivarola, J. B., and Arrua, L. A., *Appl. Catal. A* **165**, 259 (1997).
26. Centi, G., and Perathoner, S., *Appl. Catal. A* **132**, 179 (1995).
27. Burch, R., and Scire, S., *J. Phys. Chem*. **94**, 177 (1994).
28. Liu, D. J., and Robota, H. J., *Catal. Lett.* **21**, 291 (1993).
29. Texter, J., Strome, D. H., Hermann, R. G., and Klier, K., *J. Phys. Chem*. **81**, 333 (1977).
30. Ishikawa, H., Nakamura, Y., Nakayama, T., Kurusu, C., Okada, O., and Yamaguchi, R., "15th Meeting of the North American Catalysis Society." Chicago, 1997.